The interaction of oxygen with alumina-supported palladium particles

I. Meusel, J. Hoffmann, J. Hartmann, M. Heemeier, M. Bäumer, J. Libuda* and H.-J. Freund

Fritz-Haber-Institut der Max-Planck-Gesellschaft, Faradayweg 4-6, 14195 Berlin, Germany
E-mail: libuda@fhi-berlin.mpg.de

Utilizing a combination of molecular beam techniques and scanning tunneling microscopy (STM) under ultrahigh vacuum (UHV) conditions we have studied the interaction of oxygen with an alumina-supported Pd model catalyst as well as the influence of the oxygen pretreatment on the kinetics of the CO oxidation reaction. The Pd particles were deposited by metal evaporation in UHV onto a well-ordered alumina film prepared on a NiAl(110) single crystal. The particle density, morphology and structure are determined by STM both immediately after preparation and after oxygen adsorption and CO oxidation. The oxygen sticking coefficient and uptake in the temperature regime between 100 and 500 K and the kinetics of the CO oxidation reaction are quantitatively probed by molecular beam techniques. It is found that starting at temperatures below 300 K the Pd particles rapidly incorporate large amounts of oxygen, finally reaching stoichiometries of $PdO_{>0.5}$. STM shows, that neither the overall particle shape nor the dispersion is affected by the oxygen and CO treatment. Only after saturation of the bulk oxygen reservoir are stable CO oxidation conditions obtained. In the low-temperature regime (<500 K), only the surface oxygen, but not the bulk and subsurface oxygen is susceptible to the CO oxidation. The activation energies for the Langmuir–Hinshelwood step of the CO oxidation reaction were determined both in the regime of high CO coverage and high surface oxygen coverage. A comparison shows that the values are consistent with previous Pd(111) single crystal results. Thus, we conclude that, at least for the particle size under consideration in this study (5.5 nm), the LH activation energies are neither affected by the reduced size nor by the oxygen pretreatment.

KEY WORDS: palladium; alumina; oxygen; carbon monoxide; adsorption; oxidation; molecular beams; sticking coefficient; scanning tunneling microscopy

1. Introduction

The interaction of oxygen with Pd surfaces as well as the formation and influence of subsurface and bulk oxygen is a controversially discussed topic [1–25]. The remaining ambiguities in spite of the numerous studies are mainly related to the difficulties in the identification of bulk and subsurface oxygen species and the lack of quantitative adsorption and reactivity studies and the limited knowledge about the surface defect structure.

On Pd single crystal surfaces a number of studies have addressed the question of the oxygen–palladium interaction [1–18]. It was found that on Pd(111) oxygen was initially trapped in a physisorbed precursor state followed by population of a chemisorbed precursor [15]. At temperatures above 200 K the molecularly adsorbed oxygen dissociates [8]. At 300 K coverages of up to 0.25 ML (monolayers) [11] are rapidly formed, followed by a slower build-up of larger surface coverages at higher temperature [18]. There are various evidences for a slow formation of subsurface or bulk oxygen at elevated temperatures [1,3,5,6,10,12,14,16–18], which may eventually be followed or accompanied by formation of PdO [4,16]. There are contradictory observations concerning the onset of oxygen subsurface/bulk diffusion which are most likely related to the defect density of the par-

ticular Pd sample, which may strongly govern the kinetics of bulk oxygen uptake [3,5,6]. Thus, in a recent study [18] oxygen migration into the subsurface region of a Pd(111) single crystal has been observed at low temperatures (523 K) and low oxygen exposure (40 L, 1 langmuir = 10^{-6} Torr s) but has even been taken into consideration at temperatures around 300 K as well [10]. Moreover, there are indications for a rapid bulk diffusion of oxygen on small supported Pd particles [20]. The relevance of the formation of bulk and subsurface oxygen is related to the fact that such species may influence the catalytic activity, either being directly involved in the reaction or indirectly affecting the kinetics. E.g., on Pd(110) subsurface oxygen formation was discussed in relation to the kinetic oscillations in CO_2 production [14,23,24]. On Pd(111) Leisenberger et al. have recently shown that subsurface oxygen is unreactive towards adsorbed CO in the low temperature region [18].

In contrast to the single crystal surfaces, on supported metal catalysts a variety of additional kinetic effects may play a role, such as, e.g., support effects and interactions or the presence of specific adsorption or defect sites. In spite of their high relevance, equivalent studies for oxygen adsorption on supported Pd particles are extremely rare [19–22]. This is mainly due to the complexity of those systems and difficulties related to their experimental accessibility. Recently, such adsorption and reactivity studies were largely simplified by the development of supported model catalysts

---

* To whom correspondence should be addressed.

(see, e.g., [25,26]). In this work, we will employ a model catalyst which is based on a well-ordered Al_2O_3 film prepared on NiAl(110) [27,28]. Pd particles are prepared by UHV deposition of the metal under well-controlled conditions. The growth, structure and adsorption properties of the oxide film [27,28] as well as the Pd particles [26,29–32] have been subject to a number of previous studies.

In contrast to real supported catalysts, such model systems, which are prepared *in situ* under UHV conditions, largely avoid any possible contamination and provide the possibility of introducing certain features of the real catalyst without at the same time having to deal with its vast complexity. Most importantly, however, the systems remain easily accessible to many experimental techniques in surface science. In this study we take advantage of this fact and combine structural investigations using scanning tunneling microscopy (STM) with quantitative adsorption and reactivity measurements of the oxygen adsorption and its effect on the CO oxidation via molecular beam techniques. It is shown that on small particles the formation of subsurface and bulk oxygen is an highly efficient process which has to be taken into account even in kinetic studies at low reaction temperatures. In contrast to a previous study, where a reduced barrier on small particles was found [40], the activation energies for the LH reaction step agree with measurements on Pd(111) [36,37] and no influence of the reduced particle size is observed.

2. Experimental

The experiments were performed in two UHV systems. The STM apparatus is equipped with a combined atomic force/scanning tunneling microscopy system (AFM/STM, Omicron) and X-ray photoelectron spectroscopy (XPS) facilities. The sample was mounted on small carrier plates, which could be transferred between the microscopes and the main chambers containing the necessary preparation facilities. A detailed description of the system and technical details can be found elsewhere [33].

The beam experiments were performed in a new UHV molecular beam/surface spectroscopy apparatus which has been described in the literature recently [34]. The system has been specifically designed for kinetic studies an complex model systems. It offers the experimental possibility of up to three beams being crossed on the sample surface. Time- and angular-resolved as well as angular-integrated gas phase measurements can be performed and combined with time-resolved *in situ* FT-IR reflection absorption spectroscopy (IRAS). Here, we will concentrate only on the experimental details which are relevant for the integrated reactivity and sticking coefficient measurements presented in this study.

For the sticking coefficient and combined reactivity/sticking measurements the oxygen beam was generated in a supersonic expansion from a electromagnetically driven nozzle (General Valve, orifice 50 μm) at a base pressure of typically 2×10^5 Pa of high purity oxygen (AGA, >99.999%) at a gas

Table 1
Preparation conditions and structural parameters for the Pd particles on Al_2O_3/NiAl(110).

Deposition parameters	
Pd coverage (atoms cm^{-2})	2.7×10^{15}
Deposition temperature (K)	300
Deposition rate (atoms cm^{-2} s^{-1})	9×10^{12}
Structural parameters	
Island density (cm^{-2})	$1.0\ (\pm 0.2) \times 10^{12}$
Number of Pd atoms/island	$\sim$2700
Fraction of support covered by Pd	0.20 ($\pm$0.02) [35]
Fraction of surface Pd atoms	0.20 ($\pm$0.03) [35]
Island size (nm)	$\sim$5–6
Epitaxial orientation	(111)
Island structure	crystalline, predominantly (111) facets, small fraction of (100) facets

temperature of 300 K. The beam was attenuated to an intensity of typically $0.5–1 \times 10^{13}$ molecules cm^{-1} s^{-1} using a variable duty cycle mechanical chopper. The beam intensities were determined as described elsewhere [34]. For the reverse experiment, a CO (AGA, >99.996%) beam was generated from the same beam source under similar conditions (typical expansion pressure: 2×10^5 Pa, gas temperature: 300 K, beam intensity: 0.9×10^{13} molecules cm^{-1} s^{-1}). For the cycled experiments the O_2 and CO beams were generated in two effusive beam sources from backing pressures of 1 and 0.5 Pa of high purity O_2 and CO at 300 K (which was further purified using a liquid-N_2 cold trap). The beam intensities were 7.6×10^{13} and 4.0×10^{13} molecules cm^{-2} s^{-1}, respectively. Angular-integrated gas phase measurements were performed with a quadrupole mass spectrometer (ABB Extrel) which is not in line-of-sight of the sample.

Briefly, the sample was prepared by sputtering and annealing of a NiAl(110) single crystal, followed by an oxidation and annealing procedure, the details of which are given elsewhere [27,28]. The cleanliness and quality of the oxide film is checked via LEED (low-energy electron diffraction) and AES (Auger electron spectroscopy) and STM, respectively. Before the actual experiment, the active metal component (Pd, >99.9%) was deposited under well-controlled conditions by evaporation from a rod using commercial evaporators (Focus, EFM 3) based on electron bombardment. Their flux was calibrated by a quartz microbalance prior to use. During deposition, the crystal was biased with a retarding voltage in order to prevent ions from being accelerated towards the sample (point defect creation). Details concerning typical deposition rates and conditions are given in table 1.

3. Results and discussion

The growth and structure of Pd deposits as well as other metals on Al_2O_3/NiAl(110) have previously been studied over a wide range of conditions [29–32] and the results have been extensively reviewed recently [26]. In this work, we will focus on one particular set of preparation conditions (substrate temperature 300 K, Pd coverage 2.7×10^{15} atoms cm^{-2}), for which detailed information both on

the particle size and density and for the particle structure is available. In the following, we will briefly review the main features of this system. In figure 1 (a) and (b) STM images (CCT, Constant Current Topography) are shown. The Pd
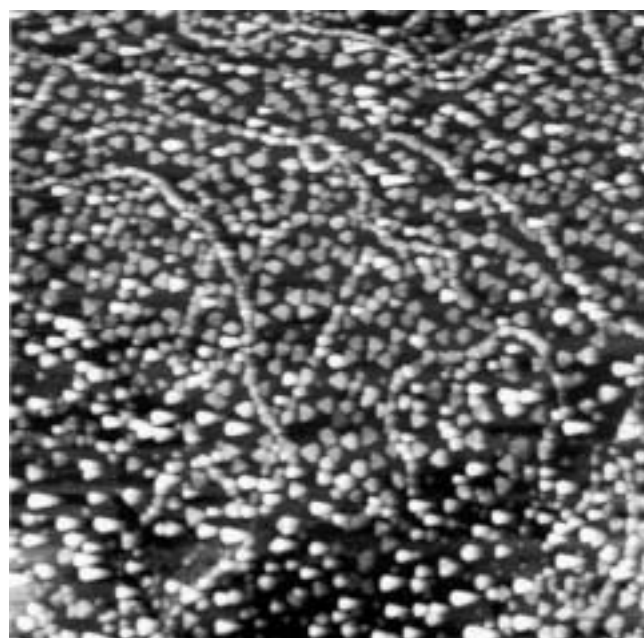
(a)
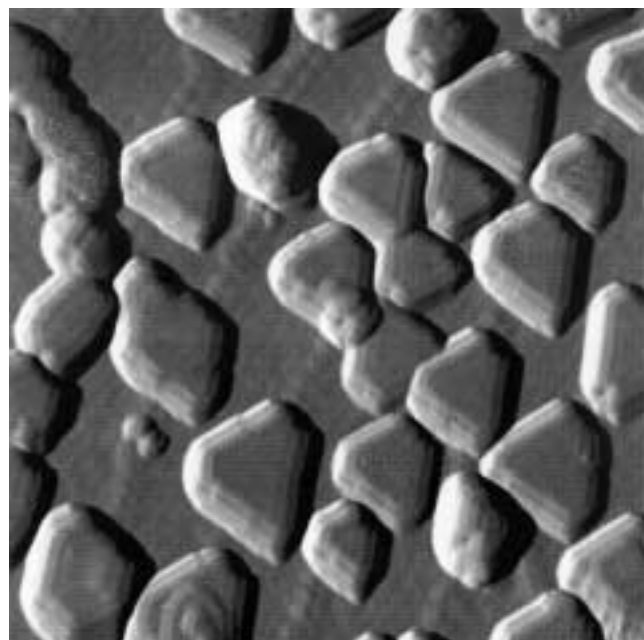
(b)
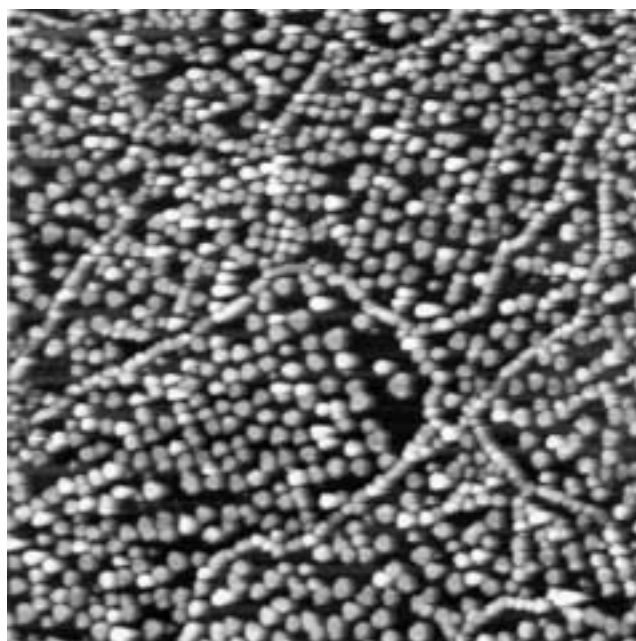
(c)
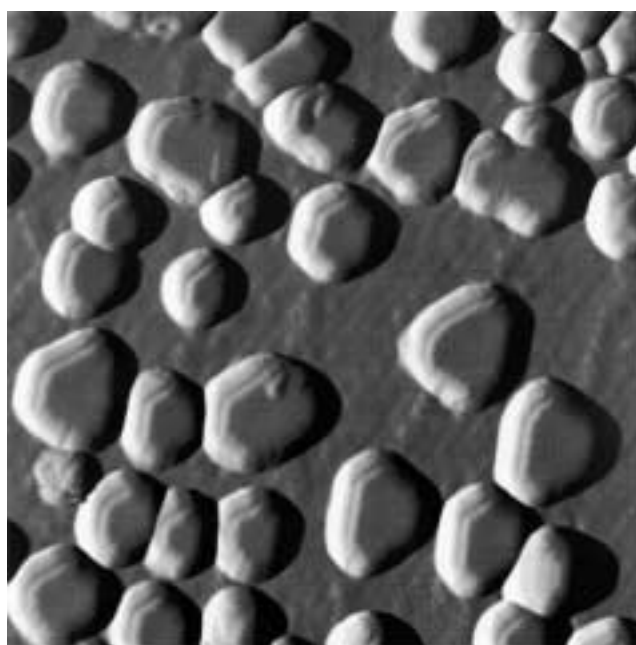
(d)
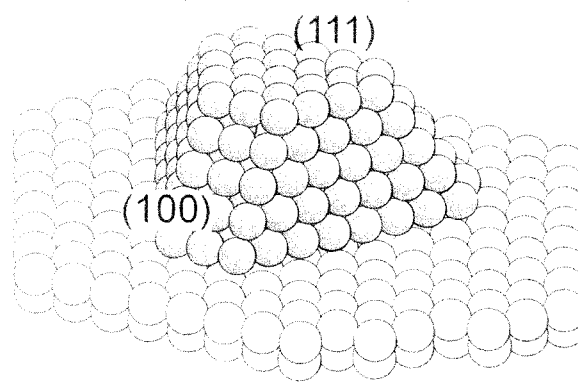
(e)

Figure 1. (a) STM image (CCT, constant current topography, 3000 Å × 3000 Å) of the Pd particles grown at 300 K on Al_2O_3/NiAl(110), after exposure to 50 L CO at 300 K; (b) differentiated close-up STM image of the Pd particles (500 Å × 500 Å), preparation as in (a); (c) STM image (CCT, 3000 Å × 3000 Å) of the Pd particles grown at 300 K on Al_2O_3/NiAl(110), after three cycles of oxygen exposure (100 L) at 400 K and subsequent CO exposure (50 L); (d) differentiated close-up STM image of the Pd particles (500 Å × 500 Å) after the same treatment as in (c); all images were taken at 300 K sample temperature; (e) schematical representation of the supported Pd particles in (b).

particles form three-dimensional islands; their density typically amounts to roughly 1×10^{13} islands cm^{-2}. From this number it can be estimated that the average Pd particle will contain about 2700 atoms, corresponding to an average particle size of approximately 5–6 nm. Please note that the islands appear larger than the above value in the STM image due to an instrumental convolution with the tip shape. Note that the apparent overlap of some particles in figure 1(b) is a result of this experimental effect. As a consequence of preferential nucleation the islands appear not to be completely homogeneously distributed over the support but will decorate oxide point and line defects (e.g., domain boundaries, see [28,29]). In the close-up shown in figure 1(b), it becomes evident that most of the Pd particles exhibit the well-defined morphology of a nanocrystallite. As indicated in the schematical representation (figure 1(e)), the particles grow in (111) orientation, preferentially exposing (111) facets and only a small fraction of (100) facets. The regular structure of the Pd crystallites has been demonstrated in a recent STM study showing atomic resolution both on the top and side facets of the particles [30]. From high resolution LEED data it was previously estimated that approximately 20% of the alumina surface is covered by the Pd particles [28,29,35]. For particles of this size and morphology, it can be estimated that the fraction of surface Pd atoms will be roughly 0.2 corresponding to a total of 0.54×10^{15} surface-Pd-atoms cm^{-2} [35]. For use in the following discussion, the information on the structural properties of the system is summarized in table 1.

In the next step we will now proceed to the CO oxidation reaction as a simple test reaction. On Pd(111) the system was early investigated by Ertl and Engel [36] using molecular beam techniques. Also, on supported model systems there are several studies, which have been extensively reviewed (see [25] and references therein). We will therefore omit a further discussion and concentrate on the question under discussion here which is the interaction and influence of oxygen.

We will start by considering an CO oxidation experiment, the results of which are displayed in figure 2: The Pd/Al$_2$O$_3$/NiAl(110) system was saturated with CO directly after preparation and heated to the reaction temperature of 366 K. Subsequently, the sample is alternately dosed with O$_2$ (7.6×10^{13} molecules cm^{-2} s^{-1}) and CO (4.0×10^{13} molecules cm^{-2} s^{-1}) via two effusive beam sources and, simultaneously, the CO$_2$ production is recorded.

First, we focus only on the first oxidation cycle: If the CO-saturated sample is exposed to the O$_2$ beam, an initially slow CO$_2$ production is observed. This is due to the low O$_2$ reactive sticking coefficient, which is further reduced due to the inhibiting effect of adsorbed CO (see, e.g., [36,37]). As the CO coverage decreases, the O$_2$ sticking coefficient and therefore the CO$_2$ production rate increases until the remaining CO coverage becomes the limiting factor. In case of the reverse experiment, there is hardly any inhibition of the CO sticking due to preadsorbed O, so that the initial increase in the CO$_2$ production rate mainly reflects the build-up of the CO concentration on the surface. If we now proceed to the
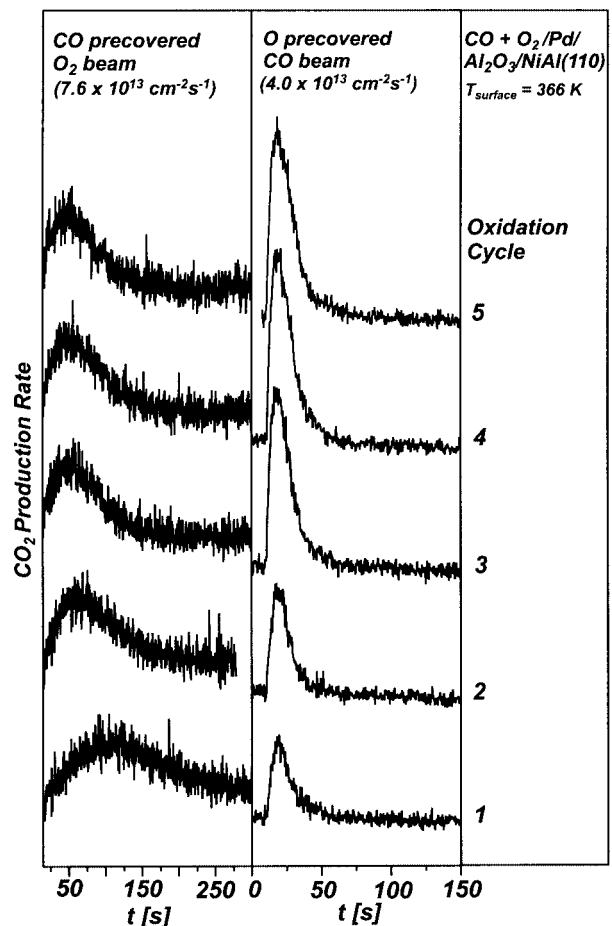
Figure 2. CO$_2$ production rate upon exposure of the CO-precovered Pd particles supported on Al$_2$O$_3$/NiAl(110) at 366 K to an O$_2$ beam (left) and of the oxygen-precovered Pd particles to a CO beam (right).

subsequent oxidation cycles, drastic changes are observed: (1) The maximum of the CO$_2$ production for the CO precovered surface is shifted to shorter times and (2) the amount of CO$_2$ deliberated from the O precovered surface increases. Only after approximately three cycles does the reaction system finally become stable and no more changes in the oxidation kinetics can be detected.

The reduced CO$_2$ production implies that initially after O$_2$ exposure less O is available to the oxidation reaction at the time when the CO beam is switched on. In the following we will show that we can exclude a major restructuring of the Pd particles upon O$_2$ exposure as a reason for this difference. Moreover, oxygen desorption can be excluded at the temperatures of the experiment [10,12,14,18]. Therefore we have to invoke an additional oxygen loss mechanism. As a possibility the subsurface diffusion of oxygen remains, which, provided the process is sufficiently fast, will lead to a depletion of the surface oxygen reservoir and a build-up of subsurface and bulk oxygen. In agreement with previous studies we may assume that the bulk and subsurface species are not susceptible to the CO oxidation reaction at low temperature [18]. A rapid subsurface diffusion is also consistent with the delayed formation of CO$_2$ from the CO-precovered sample (figure 2): although the integral amount of CO$_2$ formed
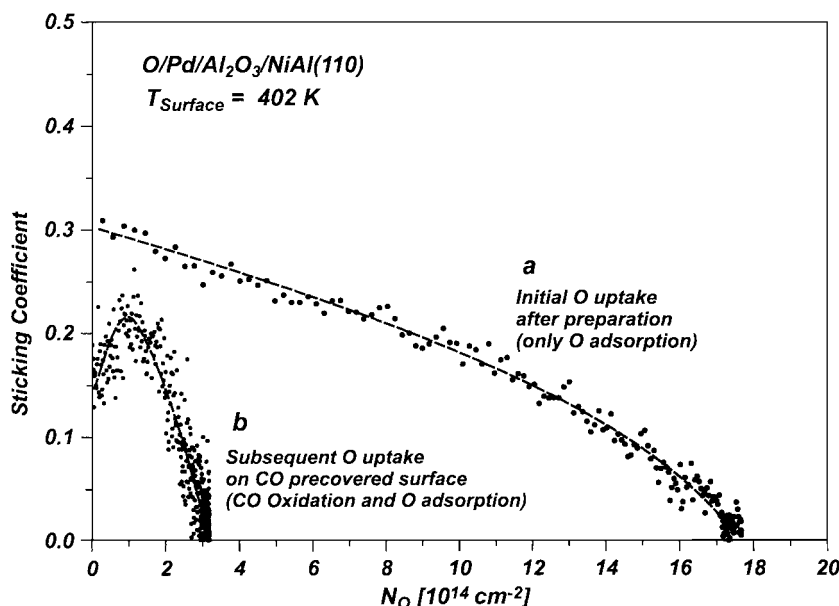
Figure 3. O_2 sticking coefficient as a function of oxygen uptake (in O-atoms cm^{-2}) at 402 K for Pd particles supported on Al$_2$O$_3$/NiAl(110) directly after preparation under UHV conditions and after several cycles of O_2 and CO exposure.

will not be affected by the subsurface and bulk oxygen formation, the additional reaction channel will compete with the CO oxidation and thus would lead to a shift of the CO$_2$ production peak.

In order to test the hypothesis of rapid oxygen subsurface and bulk diffusion, we have performed O_2 sticking coefficient measurements following the method of King and Wells [38] in a temperature range from 100 to 400 K. An example is depicted in figure 3, where we compare the sticking coefficient displayed as a function of oxygen uptake for the freshly prepared Pd sample at 402 K (figure 3(a)) and after repeated cycles of O_2 and CO exposure (figure 3(b)). First, we will consider the situation (figure 3(b)) after repeated O_2 and CO exposure. We can divide the total oxygen uptake (3.0×10^{14} O-atoms cm^{-2}) into a reactive contribution due to the CO oxidation and an adsorptive contribution. The amount of reacting O_2 will correspond to the CO precoverage, which can be estimated to be approximately 1.5×10^{14} molecules cm^{-2} from independent CO sticking coefficient measurements. Taking into account the available structural information (see table 1), this would correspond to a CO coverage (per Pd surface atom, see table 1) of $\theta \approx 0.2$–0.3, which is consistent with what would be expected for a Pd(111) surface under similar conditions (see, e.g. [2]). Consequently, we estimate the density of adsorbed atomic oxygen after the experiment to approximately 1.5×10^{14} O-atoms cm^{-2} (which would correspond to a coverage $\theta \approx 0.2$–0.3 relative to the number of Pd surface atoms, see table 1). This value appears reasonable as well, as it is known that on Pd(111) at temperatures of 300 K and above the sticking coefficient becomes extremely small at a surface coverage of $\theta = 0.25$ [11,18]. The initial increase observed in the oxygen sticking coefficient S_{O_2} is due to the CO inhibition effect mentioned before.

If we compare this result with the oxygen sticking diagram for the Pd particles initially after preparation (figure 3(a)), we find a much larger oxygen uptake in the latter case. Typically, values of approximately $1.7 \pm 0.4 \times 10^{15}$ O-atoms cm^{-2} are observed. As these values are by far too large to be compatible with pure surface adsorption we indeed have to take into account rapid surface and bulk diffusion on the time-scale of the experiment (typically 100–1000 s). Taking the reduced oxygen uptake in subsequent experiments into consideration, it becomes evident that the bulk and subsurface oxygen species do not react with adsorbed CO in this temperature region. This observation is in agreement with a recent study on Pd(111) [18].

The total oxygen uptake detectable in a King-and-Wells-type sticking coefficient measurement is plotted in figure 4 as a function of substrate temperature. Initially we find a low and slowly decreasing uptake in the temperature range between 100 and 250 K, followed by a step-like increase to a constant value of $1.7 \pm 0.4 \times 10^{15}$ O-atoms cm^{-2} in the temperature regime >300 K. Based upon previous adsorption studies, we may differentiate between three adsorption regimes (figure 4): (I) At temperatures around 100 K the adsorption process is molecular [8] at saturation coverage of $\theta = 0.62$ [11]. Taking into account the structural information (table 1), we would expect an oxygen uptake of about 3.5×10^{14} O-atoms cm^{-2}, which is consistent with the presented data. (II) At higher sample temperatures the adsorption is dissociative [8], which is connected to a reduced saturation coverage (e.g., $\theta = 0.25$ [11] on Pd(111) at 300 K). (III) In contrast to the single crystal data, the oxygen uptake at temperatures above 250 K, however, increases rapidly. The large final value of $1.7 \pm 0.4 \times 10^{15}$ O-atoms cm^{-2} can only be explained by oxygen bulk diffusion. In principle, two channels for bulk diffusion may be discussed. First, we may of course assume that the adsorbed oxygen may diffuse into the bulk
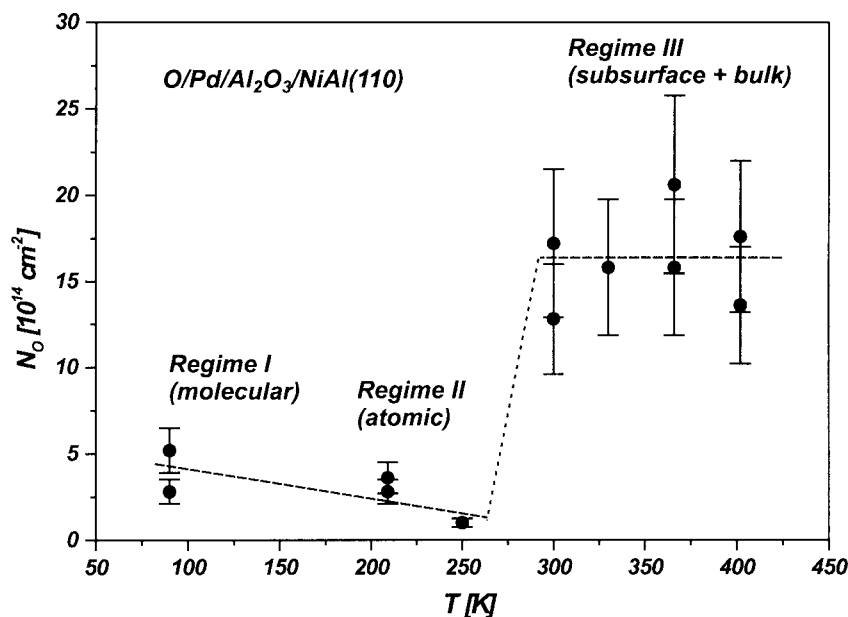
Figure 4. Oxygen uptake (in O-atoms cm^{-2}) of a sample of Pd particles supported on Al$_2$O$_3$/NiAl(110) directly after preparation under UHV conditions as a function of the sample temperature.

of the Pd particle. As discussed before this behavior appears likely for a defect-rich Pd surface. Still, we have to consider a second possibility, which is an oxygen diffusion through the alumina film, possibly mediated by adsorption on the Pd. The fact that the bulk reservoir appears to have saturation uptake independent of the sample temperature may, however, be taken as an indication that this is probably not the case. Furthermore, adsorption experiments on the clean alumina film have demonstrated that the film is inert with respect to oxygen even at large exposures, i.e., no molecular oxygen adsorbs on the oxide film under the experimental conditions applied in this work [45]. Thus it appears reasonable to assume that the alumina film indeed represents a diffusion barrier for the oxygen in this temperature region. Still, future high resolution PES (photoelectron spectroscopy) measurements are required to definitely exclude any contribution due to diffusion though the alumina film.

Following these arguments, we assume in the following discussion that the adsorbed oxygen will remain in the Pd particle. In this case, the uptake corresponds to a total stoichiometry of PdO$_{0.65\pm0.15}$ relative to the total Pd coverage. Beyond this saturation uptake, the net oxygen adsorption decreases below the detection level of the experiment.

Previously, it has been reported that supported Pd particles may undergo morphological changes induced by strongly interacting adsorbates [21]. Although the conditions are moderate in this work, we have performed STM measurements after bulk-O-saturation (i.e., after a repeated O$_2$ and CO treatment) in order to exclude such effects as a reason for the changes in adsorption behavior (figure 1 (c) and (d)). A comparison with the STM images taken before oxygen adsorption (figure 1 (a) and (b)) shows that neither the particle density nor the overall morphology of the Pd particles are affected by the large oxygen uptake. The only

detectable difference may be a slightly rounder appearance of the particle edges, which might be interpreted as an indication for distortion of the Pd lattice structure due to the incorporated oxygen. However, we have to point out again that due to tip effects and possible changes of the electronic structure the STM images are not conclusive with respect to moderate changes in the particle size. Therefore, such conclusions should be considered as preliminary. Clearly, atomically resolved STM or HR-TEM (high resolution transmission electron microscope) images are required to further elucidate the effect of the oxygen incorporation on the Pd crystallite structure.

At this point we may conclude that, starting at temperatures between 250 and 300 K, the Pd particles incorporate large amounts of oxygen on the time-scale of the sticking or reactivity experiments, finally reaching total stoichiometries of PdO$_{>0.5}$. In comparison, on single crystal surfaces this process is typically found to proceed significantly slower and is observed at higher temperatures ([18] and references therein). It has been suggested, however, that the kinetics of bulk diffusion may strongly depend on the defect density of the system [3,5,6]. This appears consistent with the present study, as in comparison with most single crystals, the supported Pd nanocrystallites in this work represent a high defect-density system. In addition to step and edge sites, we have to take into account the particle–oxide interface, where the crystallite structure may be additionally distorted due to interactions with the support. These effects may facilitate a drastically enhanced bulk diffusion for small particles, even in comparison with defective single crystal samples. Indeed, an anomalous large oxygen uptake at low temperature was previously observed for Pd supported on γ-alumina [20], although in this study no exact morphological characterization of the particles was available and no systematic tem-
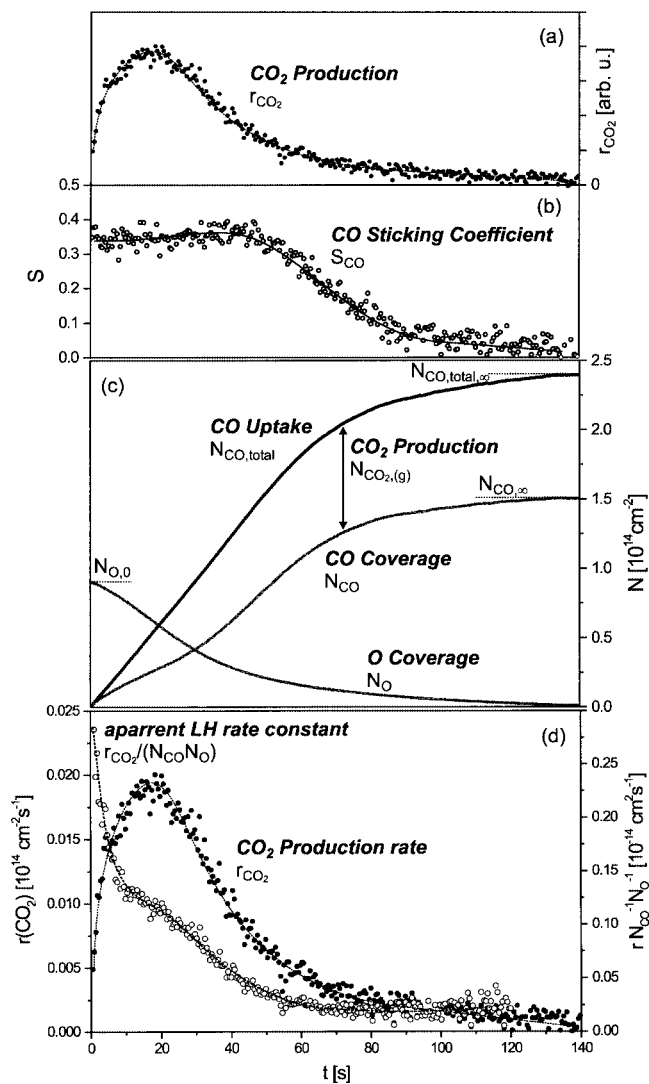
Figure 5. (a) Relative CO_2 production for O-precovered Pd/Al$_2$O$_3$/ NiAl(110) at a sample temperature of 402 K (preparation conditions 1, CO beam 8.6 × 10^{12} molecules cm^{-2} s^{-1}), (b) CO sticking coefficient as a function of experiment time; (c) O and CO surface coverages (see text); (d) absolute CO_2 production rate and apparent Langmuir–Hinshelwood rate constant.

ing coefficient and the CO_2 production rate. An example is displayed in figure 5, where the oxygen-precovered surface was exposed to the CO beam (supersonic beam source, 8.6 × 10^{12} molecules cm^{-2} s^{-1}). From a simultaneous measurement of the CO sticking coefficient (figure 5(a)) and the CO_2 production rate (figure 5(b)), it is straightforward to determine the absolute reaction rate as a function of the oxygen coverage N_O and CO coverage N_{CO}.

Briefly, total CO uptake $N_{CO,total,\infty}$ is determined by integration of the CO sticking coefficient (figure 5(b)). This value represents the sum of two channels, CO adsorption and CO oxidation. The final amount of adsorbed CO $N_{CO,\infty}$ can be estimated from a separate measurement after thermal desorption of the CO. The remaining amount of CO corresponds to the reaction channel and is equal to the initial oxygen precoverage $N_{O,0}$. Once these limiting values are known, the oxygen and CO coverages at any time t can be determined by integration of the CO sticking coefficient and CO_2 production rate, respectively. A detailed description of the procedure can be found in the literature [36,40,42]. The results for the experiment shown in figure 5 (a) and (b) are displayed in figure 5(c). Please note that due to the low reaction temperatures, there is substantial coadsorption of O and CO. We may now apply a rigorous definition of the Langmuir–Hinshelwood (LH) rate equation as

$$\frac{\mathrm{d}}{\mathrm{d}t} N_{CO_2(g)} = k_{N_{CO}, N_O} N_{CO} N_O$$

to derive the rate constant k_{N_{CO}, N_O}. It has to be pointed out that in such a definition, the rate constant may strongly depend on the adsorbate coverages, e.g. due to energetic effects related to intermolecular interaction but also due to the spatial distribution of the adsorbates. The result is plotted in figure 5(d). The origin of the initially strongly increased rate constant is not clear yet [42], but may be either related to the presence of different facets or defect sites or to the formation of more densely packed O-layers, which have been proposed to exhibit an increased reactivity on Pd(100) and Pd(111) films [43,44].

Here, we will not further discuss this question, but in an attempt to compare the kinetics of the LH step on the oxygen-saturated particles to previous measurements on clean single crystal surfaces, we proceed to a determination of the activation barriers. For this purpose we have performed two series of experiments equivalent to the one displayed in figure 5. In the first series we start from the CO-saturated system and determine the rate constant at various temperatures between 350 and 450 K. This procedure will yield reliable rate constants in the limit of high CO and lower O coverage. Note that in principle also the rate constants at low CO coverage can be determined from these measurements, due to the low reaction rate and uncertainties in the coverage determination, however, these numbers are prone to artifacts and are omitted here. Once the rate constants

perature dependence was reported. In view of these results it becomes evident that studying the kinetics of a test reaction such as the CO oxidation on supported nanoparticles, we have to explicitly take into account the influence of bulk diffusion, even at low reaction temperatures.

Following the qualitative discussion above, we will therefore reconsider the CO oxidation from a more quantitative point of view. Using molecular beam methods, the reaction has been studied both on single crystal Pd surfaces [36, 37,39] and on supported Pd particles [20,25,40,41]. Here, we will consider the reaction kinetics on the fully oxygen-saturated system, i.e., the conditions on which the model catalyst was observed to show constant oxidation rates in figure 2. We take advantage of the single scattering conditions of the molecular beam experiment, which allow us to perform a simultaneous measurement of the reactants stick-

Figure 6. Langmuir–Hinshelwood activation energy for the oxidation of CO on Pd particles supported on $Al_2O_3/NiAl(110)$ after oxygen saturation. The data was derived from a series of experiments equivalent to the one shown in figure 5 over a temperature range from 350 to 450 K. The experiments were performed either exposing a CO-precovered sample to an O_2 beam (a) or exposing an oxygen-precovered sample to a CO beam (b).

are known we may attempt to determine the LH activation energy,

$$E_{a,\text{LH}} = \left(\frac{d}{dT^{-1}} \ln k_{N_{CO},N_O} \right)_{N_{CO},N_O=\text{const.}}.$$

As in the current set of experiments the CO and the O coverage are no independent parameters, we may in a first step determine the activation energy as a function of CO coverage. Subsequently, we consider the limiting case of high CO and low O coverage so that we can neglect the influence of possible variations in the O coverage at different reaction temperatures. As shown in figure 6(a), we derive under these conditions an activation barrier of 57 ± 8 kJ mol^{-1}. Additionally, we can perform the reverse experiment, i.e., we expose the oxygen-precovered sample to a CO beam. Thus we determine the activation barrier, this time in the limiting case of high oxygen and low CO coverage. As shown in figure 6(b), in this case we derive a value of 62 ± 9 kJ mol^{-1}.

In spite of the vast number of studies on the CO oxidation on Pd, there are only few measurements of the activation energy under comparable conditions and using similar methods. On Pd(111) Engel and Ertl have determined activation energies of 25 kcal mol^{-1} (105 kJ mol^{-1}) at high reaction temperatures (>500 K) and low oxygen coverage, which decreases to 14 ± 2 kcal mol^{-1} (59 ± 8 kJ mol^{-1}) at lower reaction temperature (<420 K) and high oxygen coverage [36,37]. This effect was related to adsorbate interactions at higher coverage, which give rise to a decreasing adsorption energy and thus also to a decreasing effective activation barrier. In a study applying a similar experimental approach to not only single crystal surfaces but also supported Pd particles, a strongly decreased activation energy was found for smaller Pd particles (particle diameter 27 and 2.5 nm) [40].

It has to be concluded that the present result does not confirm the hypothesis of a reduced activation barrier for the small Pd particles (5–6 nm) under investigation in this study. Moreover, it is noteworthy that the activation energies are in excellent agreement with the activation barrier determined in the low temperature regime for Pd(111) [36,37]. Although this may not have been explicitly checked in the mentioned study [36], we may anticipate that subsurface and bulk oxygen formation play a less important role in kinetic studies on the close-packed Pd(111) surface. This, however, would mean that the large oxygen uptake of the Pd nanoparticles may only have a minor influence on the kinetics of the CO oxidation reaction. In future studies this conclusion will have to be tested employing experimental techniques which allow a direct and quantitative detection of subsurface oxygen species in combination with a well-controlled variation of the structural parameters of the Pd deposits.

4. Conclusions

In conclusion, we have prepared and characterized a Pd supported model catalyst system, based on an well-ordered Al_2O_3 film prepared on NiAl(110). The growth and morphology of the Pd particles were investigated by STM, yielding a particle density of approximately 1×10^{13} islands cm^{-2} and an average particle size of 5–6 nm. The particles exhibit a crystalline structure, preferentially exposing (111) facets.

Using molecular beam techniques, we have probed the model system with respect to its interaction with O_2 as well as with respect to the kinetics of the CO oxidation reaction in the temperature region between 350 and 450 K. It is found that the Pd particles rapidly incorporate large amounts of oxygen starting at sample temperatures as low as 250–300 K. The oxygen uptake saturates only at stoichiometries of PdO$_{>0.5}$. STM investigations demonstrate that neither the density nor the overall morphology of the Pd particles is affected by the bulk oxygen formation.

Measurements of the CO oxidation rate using molecular beam methods show that due to the rapid oxygen incorporation stable oxidation rates are only reached after saturation

of the bulk reservoir. Finally, we have determined the activation barriers for the CO oxidation reaction in the limit of large oxygen coverage and large CO coverage, respectively. The values are consistent with previous measurements on Pd(111), indicating the presence of the subsurface/bulk oxygen has only a minor influence on the activation barrier of the reaction.

Acknowledgement

References

[1] H. Conrad, G. Ertl, J. Küppers and E.E. Latta, Surf. Sci. 65 (1977) 254.
[2] T. Engel, J. Chem. Phys. 69 (1978) 373.
[3] D.L. Weissman, M.L. Shek and W.E. Spicer, Surf. Sci. 92 (1980) L59.
[4] P. Legare, L. Hilaire, G. Maire, G. Krill and A. Amamou, Surf. Sci. 107 (1981) 533.
[5] D.L. Weissman-Wenicur, M.L. Shek, P.M. Stefan, I. Lindau and W.E. Spicer, Surf. Sci. 127 (1983) 513.
[6] L. Surnev, G. Bliznakov and M. Kiskinova, Surf. Sci. 140 (1984) 249.
[7] T. Matsushima, Surf. Sci. 157 (1985) 297.
[8] R. Imbihl and J.E. Demuth, Surf. Sci. 173 (1986) 395.
[9] B. Oral and R.W. Vook, Appl. Surf. Sci. 29 (1987) 20.
[10] M. Milun, P. Pervan, M. Vacjic and K. Wandelt, Surf. Sci. 211–212 (1989) 887.
[11] X. Guo, A. Hoffman and J.T. Yates, Jr., J. Chem. Phys. 90 (1989) 5787.
[12] B.A. Banse and B.E. Koel, Surf. Sci. 232 (1990) 275.
[13] G.W. Simmons, Y.-N. Wang, J. Marcos and K. Klier, J. Phys. Chem. 95 (1991) 4522.
[14] V.A. Bondzie, P. Kleban and D.J. Dwyer, Surf. Sci. 347 (1996) 319.
[15] P. Sjövall and P. Uvdal, Chem. Phys. Lett. 282 (1998) 355; J. Vac. Sci. Technol. A 16 (1998) 943.
[16] E.H. Voogt, A.J.M. Mens, O.L.J. Gijzeman and J.W. Geus, Surf. Sci. 373 (1997) 210.
[17] W. Huang, R. Zhai and W. Bao, Surf. Sci. 439 (1999) L803.
[18] F.P. Leisenberger, G. Koller, M. Sock, S. Surnev, M.G. Ramsey, F.P. Netzer, B. Klötzer and K. Hayek, Surf. Sci. 445 (2000) 380.
[19] M. Eriksson and L.G. Petersson, Surf. Sci. 311 (1994) 139.
[20] I. Stará, V. Nehasil and V. Matolín, Surf. Sci. 365 (1996) 69.
[21] H. Graoui, S. Giorgio and C.R. Henry, Surf. Sci. 417 (1998) 350.
[22] M. Eriksson, L. Olsson, U. Helmersson, R. Erlandsson and L.-G. Ekedahl, Thin Solid Films 342 (1999) 297.
[23] S. Ladas, R. Imbihl and G. Ertl, Surf. Sci. 219 (1989) 88.
[24] M.R. Bassett and R. Imbihl, J. Chem. Phys. 93 (1990) 811.
[25] C.R. Henry, Surf. Sci. Rep. 31 (1998) 121.
[26] M. Bäumer and H.-J. Freund, Prog. Surf. Sci. 61 (1999) 127.
[27] R.M. Jaeger, H. Kuhlenbeck, H.-J. Freund, M. Wuttig, W. Hoffmann, R. Franchy and H. Ibach, Surf. Sci. 259 (1991) 235.
[28] J. Libuda, F. Winkelmann, M. Bäumer, H.-J. Freund, Th. Bertrams, H. Neddermeyer and K. Müller, Surf. Sci. 318 (1994) 61.
[29] M. Bäumer, J. Libuda and H.-J. Freund, in: *Chemisorption and Reactivity on Supported Clusters and Thin Films*, NATO Advanced Study Institute, NATO ASI Ser. E, eds. M. Lambert and G. Pacchioni (Kluwer Academic, Dordrecht, 1997) p. 61.
[30] K.H. Hansen, T. Worren, S. Stempel, E. Laegsgaard, M. Bäumer, H.-J. Freund, F. Besenbacher and I. Stensgaard I, Phys. Rev. Lett. 83 (1999) 4120.
[31] M. Bäumer, J. Libuda, A. Sandell, H.-J. Freund, G. Graw, T. Bertrams and H. Neddermeyer, Ber. Bunsenges. Phys. Chem. 99 (1995) 1381.
[32] K. Wolter, O. Seiferth, H. Kuhlenbeck, M. Bäumer and H.-J. Freund, Surf. Sci. 399 (1998) 190.
[33] M. Bäumer, M. Frank, J. Libuda, S. Stempel and H.-J. Freund, Surf. Sci. 391 (1997) 204;
S. Stempel, Ph.D. thesis, Berlin (1998).
[34] J. Libuda, I. Meusel, J. Hartmann and H.-J. Freund, Rev. Sci. Instrum., submitted.
[35] J. Libuda, Ph.D. thesis, Bochum (1996).
[36] T. Engel and G. Ertl, J. Phys. Chem. 69 (1978) 1267.
[37] T. Engel and G. Ertl, in: *The Chemical Physics of Solid Surfaces and Heterogeneous Catalysis*, Vol. 4, eds. D.A. King and D.P. Woodruff (Elsevier, 1982) p. 73.
[38] D.A. King and M.G. Wells, Proc. Roy. Soc. London A 339 (1974) 245; Surf. Sci. 29 (1972) 454.
[39] I.Z. Jones, R.A. Bennett and M. Bowker, Surf. Sci. 439 (1999) 235.
[40] I. Stará, V. Nehasil and V. Matolín, Surf. Sci. 331–333 (1995) 173.
[41] C. Becker and C.R. Henry, Surf. Sci. 352 (1996) 457; Catal. Lett. 43 (1997) 55.
[42] T. Dellwig, J. Hartmann, J. Libuda, I. Meusel, G. Rupprecht, H. Unterhalt and H.-J. Freund, Topics Catal., in press.
[43] H. Fornander, L.-G. Ekedahl and H. Dannetun, Catal. Lett. 59 (1999) 107.
[44] H. Fornander, H. Dannetun and L.-G. Ekedahl, Surf. Sci. 440 (1999) 375.
[45] R.M. Jaeger, Ph.D. thesis, Bochum (1992).